Nonprehensile Dynamic Manipulation of a Sheet-like Viscoelastic Object

Ixchel G. Ramirez-Alpizar, Mitsuru Higashimori, Makoto Kaneko, Chia-Hung Tsai, and Imin Kao

***Abstract*— This paper discusses a nonprehensile dynamic manipulation of a deformable object, where the object is remotely manipulated on a plate attached at the tip of a bar. We have found that the object's deformation generated by dynamic effects can drastically contribute to a fast and stable object rotation. We introduce a new simulation model for a sheet-like object, where the object is constructed of multiple nodes connected by three DOFs viscoelastic joint units. We apply the model to real food after the viscoelastic parameters are estimated. Then, simulation analysis is used to show how the object's rotation behavior changes with respect to the plate's motion frequency, similar to the motion of human legs sliding, walking, and running. Finally we obtain an optimum plate motion leading to the maximal angular velocity of the object. We also reveal that an appropriate angular acceleration of the plate is essential for a dynamically stable and fast object rotation.**

I. Introduction

Along with the advance of technology in both sensing and actuation, dynamic skills in robotics have been developed in [1]–[3]. In the case where a simple end-effector is used, a robot-system can compensate for its lack of DOFs (degrees of freedom) by utilizing dynamic effects produced by high-speed robot motions and by using an appropriate manipulation strategy. Based on the above discussion, our former works treated a dynamic manipulation inspired by the handling of a pizza peel [4], as shown in Fig. 1. A chef handles the peel and remotely manipulates a pizza on the plate. We found that the chef aggressively utilizes two DOFs from the remote handling location during the manipulation: translation X along the bar and rotation Θ around the bar. We have proposed a nonprehensile dynamic manipulation for controlling the position and the orientation of an object on a plate by applying the peel mechanism to the robot system. This manipulation scheme has the advantage that the robot can remotely manipulate an object in areas with high temperatures, electromagnetic fields, etc, where electrical hardware is unavailable. We have also found that a deformable object can rotate faster than a rigid one [5], as shown in Fig. 1(a) and (b). In order to extend the aforementioned investigation, we clarify what actually happens in the manipulation of a deformable object, and obtain an optimum plate motion towards an effective manipulation.

I. Ramirez-Alpizar, M. Higashimori, and M. Kaneko are with the Department of Mechanical Engineering, Graduate School of Engineering, Osaka University, 2-1 Yamadaoka, Suita, 565-0871, Japan ixchel@hh.mech.eng.osaka-u.ac.jp, {higashi, kaneko}@mech.eng.osaka-u.ac.jp

C. Tsai and I. Kao are with the Department of Mechanical Engineering, State University of New York (SUNY) at Stony Brook, Stony Brook, NY 11794-2300, USA tsai@mal.eng.sunysb.edu, ikao@ms.cc.sunysb.edu

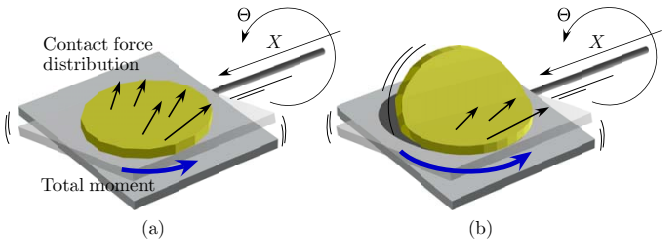

Fig. 1. A nonprehensile manipulation for rotating an object: with a rigid body in (a) and a deformable body in (b).

In this paper, we introduce a new model for approximating dynamic characteristics of a sheet-like deformable object on the plate. This model is composed of multiple nodes with mass, where neighboring nodes are connected each other by what we call a viscoelastic joint unit. This unit is composed of three joints: bending, compression/tension, and torsion. While the bending and the compression joints have viscoelastic elements, the torsion joint is free. After estimating the viscoelastic parameters of real food, we show the simulation results where the dynamic behavior of the object nicely corresponds to that in experiments. Through simulation analysis, we show that the object's rotation behavior changes with respect to the plate's motion frequency, similar to sliding, walking, and running motions done by human legs. We finally reveal that an optimum point leading to the maximal rotational speed of the object exists and depends upon the angular acceleration of the plate.

This paper is organized as follows: In section II, we briefly review the related works. In section III, we show basic experiments. In section IV, we introduce a simulation model for a deformable object. In section V, we show how to estimate the viscoelastic parameters of the object. In section VI, we show the simulation results based on real food. In section VII, we give the conclusion of this work.

II. Related Works

There have been various works discussing nonprehensile manipulation. Arai *et al.* have discussed a manipulation strategy where a cube is rotated around its edge on a plate attached at the tip of a six DOFs manipulator [1]. Lynch *et al.* have discussed controllability, motion planning, and implementation of a planar dynamic nonprehensile manipulation [2]. Various dynamic tasks were performed by using a single joint manipulator. Those tasks include snatching an object from a table, rolling an object on the surface of an arm, and throwing and catching it. Amagai *et al.* have shown the experiments where an object is manipulated on a plate

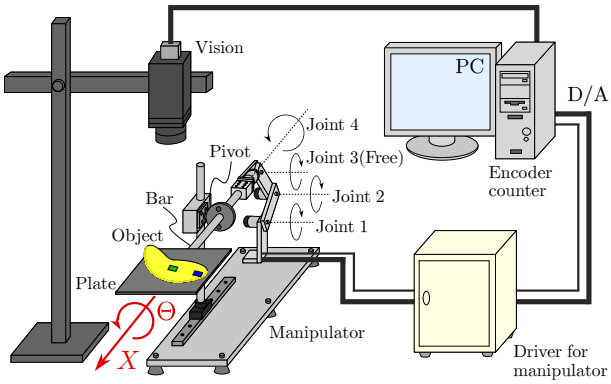

Fig. 2. An overview of the experimental system.

attached at the tip of a six DOFs manipulator based on visual information [3]. Reznik and Canny have developed the Universal Planar Manipulator (UPM) based on a single horizontally-vibrating plate with three DOFs [6]. They have demonstrated that multiple objects were simultaneously moved toward target directions. Böhringer *et al.* [7] have discussed algorithms for sensorless positioning and orienting of planar parts using different vibration patterns. Vose *et al.* [8] have discussed sensorless control methods for point parts sliding on a rigid plate with a vibration around an arbitrary axis. Most of the works done on manipulation utilizing a plate have supposed that the object is rigid.

III. Experiment

Fig. 2 shows an overview of the experimental system [4]. A plate is attached at the tip of a manipulator and a vision system observes the object on the plate. The manipulator possesses three active joints and a free joint. The plate of 100 mm $\times$ 100 mm fixed at the tip of the bar moves along the longitudinal axis of it (translational DOF: X) by the rotations of the 1st and the 2nd joints. The plate rotates around the longitudinal axis of the bar (rotational DOF: Θ) by the rotation of the 4th joint. A small circular pancake is utilized as a deformable object. It has a mass of 10 g, a radius of 42 mm, and a thickness of 1.0 mm. Additionally, as a rigid body, we prepare another object made of plastic with the same physical properties except for the bending stiffness.

We give to the plate's two DOFs of motion the sinusoid trajectories given by $X(t) = 2\sin(14\pi t)$ mm and $\Theta(t) = -A_p \sin(14\pi t)$ deg. The object rotates continuously on the plate by cyclically changing the friction force distribution. For details about the principle of rotating the object, see [4]. Fig. 3 shows a series of photos showing the rotational motion of the rigid object where the amplitude of Θ is given by $A_p = 16$ deg. From Fig. 3, it can be seen that the object does not bend and a full contact between the plate and the object is kept. The object rotates with an angular velocity of 15.7 deg/s. Moreover, if we give an amplitude larger than $A_p = 16$ deg, the object falls from the plate. On the contrary, Fig. 4 shows a series of photos showing the rotational motion of the deformable object where the amplitude of Θ is given by $A_p = 24$ deg. From Fig. 4, it can be seen that the object

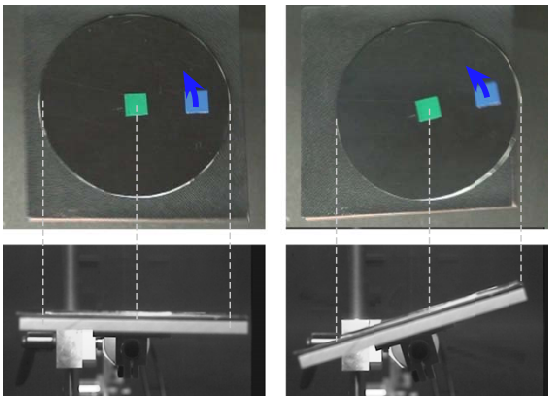

(a) $t = 0.14$[s] (b) $t = 0.54$[s]

Fig. 3. Rotatinal motion of a rigid object: the object is rotating with an angular velocity of 15.7 deg/s.

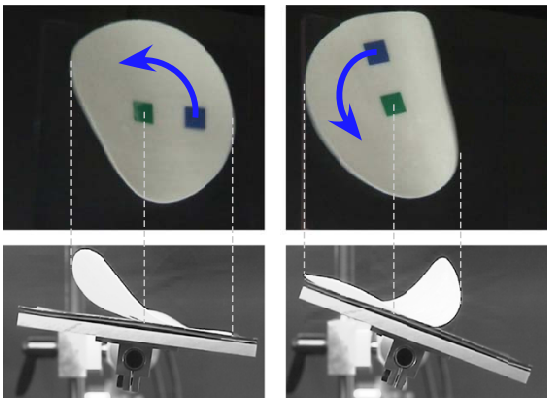

(a) $t = 0.21$[s] (b) $t = 0.61$[s]

Fig. 4. Rotatinal motion of a deformable object: the object is rotating with an angular velocity of 251 deg/s.

is bent by the inertial force given by the plate, thus the contact area between the plate and the object is decreased. This object's behavior works effectively for decreasing the brake torque. As a result, the deformable object can rotate faster than the rigid object on the plate. The object rotates with an angular velocity of 251.7 deg/s, which is 16 times faster than the rigid object. It is remarkable that the behavior of the deformable object during the rotation is similar to a human or a biped robot stepping on the floor. We observed that the DOF of Θ is effective for giving to the deformable object a role of legs for generating step motions.

IV. Modeling

We introduce a viscoelastic model for expressing dynamic behaviors of a sheet-like deformable object on a plate.

Assumptions: Consider a plate and a sheet-like deformable object as shown in Fig. 1. To simplify the analysis, we set the following assumptions:

1: The plate is rigid.
2: The object is deformable and its thickness is small.
3: The object is isotropic and it has uniform mass distribution and uniform viscoelasticity.
4: The friction coefficient between the plate and the object

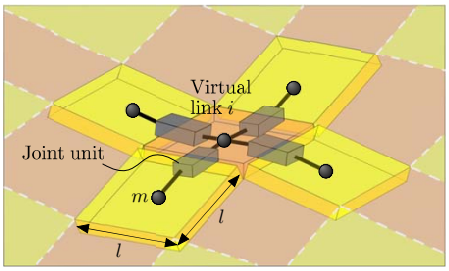

(a) Object model

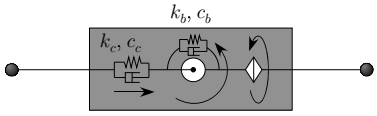

(b) Three-DOFs joint unit

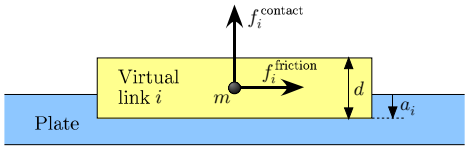

(c) Contact model

Fig. 5. Deformable object model.

based on Coulomb's law is uniform and is given by μ_s and μ_k for static and dynamic coefficients, respectively.

Deformable object model: For a sheet-like deformable object, we consider virtual tile links as shown in Fig. 5(a). The link is a square with sides of lengh l. Based on the shape and the size of the modeled object, the arrangement of virtual tiles is determined. A node with a mass of m is located at the center of the link, where neighboring nodes are connected each other by a viscoelastic joint unit as shown in Fig. 5(b). The joint unit is composed of three DOFs: bending, compression/tension, and torsion. While the bending and the compression joints have viscoelastic elements given by a Kelvin-Voigt model, the torsion joint is completely free. In Fig. 5(b), k_b and c_b express the elasticity and viscosity of the bending joint, respectively. Also, k_c and c_c are the elasticity and viscosity of the compression joint, respectively.

Contact Model: Fig. 5(c) shows the contact model between the plate and the i-th virtual link. The contact force is calculated with the penalty method based on the Kelvin-Voigt model [10]. The contact force f_i^{contact} applied to the node is given by

$$f_i^{\text{contact}} = k_{\text{contact}} a_i^{2.2} + c_{\text{contact}} \dot{a}_i \quad (a_i \geq 0) \tag{1}$$

where a_i, k_{contact}, and c_{contact} are the distance between the surface of the plate and the surface of the virtual link, the elasticity, and the viscosity, respectively. Also, the friction force f_i^{friction} applied to the node is given by,

$$f_i^{\text{friction}} = \mu f_i^{\text{contact}} \quad (\mu = \mu_k \text{ or } \mu_s) \tag{2}$$

where f_i^{friction} is in opposite direction to the relative velocity of the node with respect to the plate's surface.

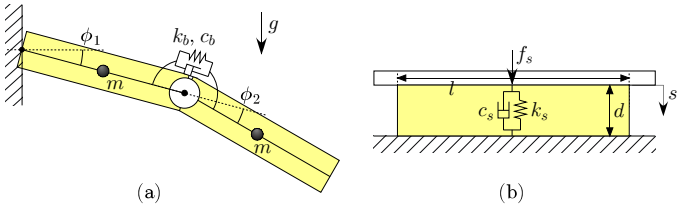

Fig. 6. Parameter estimation model.

V. Parameter Estimation

We show how to estimate the viscoelastic parameters of a real deformable object by experiments.

A. How to Estimate Parameters

Viscoelasticity in Bending: Fig. 6(a) shows the model utilized to estimate the viscoelasticity in bending. This model is composed of two links connected by a single joint, where one tip is fixed and the other is free; thus, it is deformed by gravity. This deformation is approximated by two angles: ϕ_1 and ϕ_2, which denote the angle of the fixed point and the one of the joint located at the center, respectively. The equation of motion of this model is expressed as follows,

$$\begin{bmatrix} \dot{\phi}_2 & \phi_2 \end{bmatrix} \begin{bmatrix} c_b \\ k_b \end{bmatrix} = \frac{1}{2} mgl \cos(\phi_1 + \phi_2) - \frac{1}{4} ml^2 \ddot{\phi}_2 \tag{3}$$

Using the sampling data in $t_1 \leq t \leq t_n$, (3) is expressed by

$$\boldsymbol{A}\boldsymbol{p}_b = \boldsymbol{q} \tag{4}$$

where

$$\boldsymbol{A} \triangleq \begin{bmatrix} \dot{\phi}_2(t_1) & \phi_2(t_1) \\ \dot{\phi}_2(t_2) & \phi_2(t_2) \\ \vdots & \vdots \\ \dot{\phi}_2(t_n) & \phi_2(t_n) \end{bmatrix}, \quad \boldsymbol{p}_b \triangleq \begin{bmatrix} c_b & k_b \end{bmatrix}^{\mathrm{T}},$$

$$\boldsymbol{q} \triangleq \begin{bmatrix} \frac{1}{2} mgl \cos(\phi_1(t_1) + \phi_2(t_1)) - \frac{1}{4} ml^2 \ddot{\phi}_2(t_1) \\ \frac{1}{2} mgl \cos(\phi_1(t_2) + \phi_2(t_2)) - \frac{1}{4} ml^2 \ddot{\phi}_2(t_2) \\ \vdots \\ \frac{1}{2} mgl \cos(\phi_1(t_n) + \phi_2(t_n)) - \frac{1}{4} ml^2 \ddot{\phi}_2(t_n) \end{bmatrix}$$

From the least squares solution of (4), the viscoelastic parameters $\hat{\boldsymbol{p}}_b \triangleq [\hat{c}_b \ \hat{k}_b]^{\mathrm{T}}$ can be estimated by

$$\hat{\boldsymbol{p}}_b = (\boldsymbol{A}^{\mathrm{T}}\boldsymbol{A})^{-1}\boldsymbol{A}^{\mathrm{T}}\boldsymbol{q} \tag{5}$$

Viscoelasticity in Compression: Fig. 6(b) shows the model utilized to estimate the viscoelasticity in compression, where one link with a small thickness d is put on the table. The deformation of the link is given by a displacement s, and the viscoelastic parameters in the Kelvin-Voigt model are k_s, c_s. The contact force f_s applied to the surface $l \times l$ and the displacement s are utilized in the equation of motion which is expressed as follows,

$$\begin{bmatrix} \dot{s} & s \end{bmatrix} \begin{bmatrix} c_s \\ k_s \end{bmatrix} = f_s \tag{6}$$

Using the sampling data in $t_1 \leq t \leq t_n$, (6) is expressed by

$$\boldsymbol{B}\boldsymbol{p}_s = \boldsymbol{f}_s \tag{7}$$

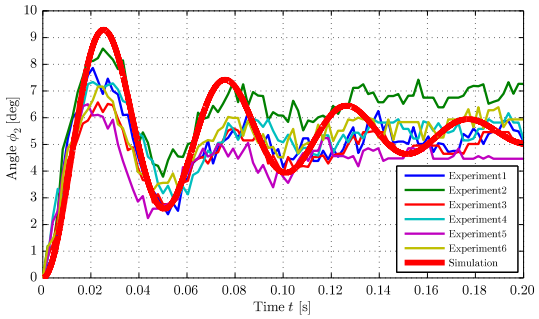

Fig. 7. Angle ϕ_2 with respect to time during the estimation of the viscoelasticity in bending.

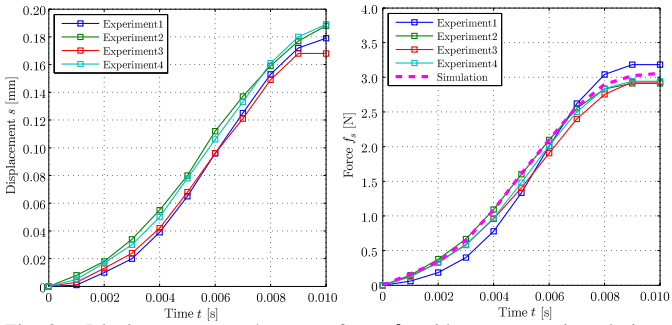

Fig. 8. Displacement s and contact force f_p with respect to time during the estimation of the viscoelasticity in compression.

where

$$\boldsymbol{B} \triangleq \begin{bmatrix} \dot{s}(t_1) & s(t_1) \\ \dot{s}(t_2) & s(t_2) \\ \vdots & \vdots \\ \dot{s}(t_n) & s(t_n) \end{bmatrix}, \quad \boldsymbol{p}_s \triangleq \begin{bmatrix} c_s & k_s \end{bmatrix}^{\mathrm{T}},$$
$$\boldsymbol{f}_s \triangleq \begin{bmatrix} f_s(t_1) & \cdots & f_s(t_n) \end{bmatrix}^{\mathrm{T}}$$

From the least squares solution of (7), the viscoelastic parameters $\hat{\boldsymbol{p}}_s \triangleq [\hat{c}_s \ \hat{k}_s]^{\mathrm{T}}$ can be estimated by

$$\hat{\boldsymbol{p}}_s = (\boldsymbol{B}^{\mathrm{T}}\boldsymbol{B})^{-1}\boldsymbol{B}^{\mathrm{T}}\boldsymbol{f}_s \tag{8}$$

By converting $\hat{\boldsymbol{p}}_s$, $\hat{\boldsymbol{p}}_c \triangleq [\hat{c}_c \ \hat{k}_c]^{\mathrm{T}}$ can be obtained by

$$\hat{\boldsymbol{p}}_c = \hat{\boldsymbol{p}}_s \, (d/l)^2 \tag{9}$$

which expresses the viscoelasticity for a contact force applied to the surface $l \times d$ with thickness l.

B. Parameter Estimation in a Real Object

As a real deformable object, a slice of cheese is utilized in the experiment, where each link is given by $l = 10$ mm, $d = 2.5$ mm, and $m = 0.285$ g. Fig. 7 shows the angle ϕ_2 with respect to time during the deformation by gravity. From these data and (5), $\hat{k}_b = 2.72 \times 10^{-3}$ Nmm/deg, $\hat{c}_b = 4.23 \times 10^{-6}$ Nmm/(deg/s) are obtained. In Fig. 7, the reconstructed result of ϕ_2 using the estimated parameters is overlapped. From this figure, it can be seen that the experimental results and the reconstructed one matched nicely. Fig. 8 shows the displacement s and the contact force f_s with respect to time during the deformation by compression. From these data and (8), $\hat{k}_s = 12$ N/mm and $\hat{c}_s = 7.9 \times 10^{-3}$ N/(mm/s) are obtained. Also, $\hat{k}_c = 0.79$ N/mm and $\hat{c}_c = 4.9 \times 10^{-4}$ N/(mm/s) are obtained by the conversion based on (9) . In Fig. 8, the reconstructed result of f_s using the estimated parameters and the displacement in Experiment 1 is overlapped. From this figure, it can be seen that the experimental results and the reconstructed one matched nicely.

VI. Simulation Based on Real Food

A. Simulation Setting

The object is a circular slice of cheese which has radius $r = 40$ mm, thickness $d = 2.5$ mm, and mass $M = 13.6$ g. The simulation software MD Adams (MSC.Software Corp.) is utilized for computing the dynamic motion of the object. The simulation model as shown in Fig. 9 is composed of 52 links with $l = 10$ mm. The four viscoelastic parameters obtained in the previous section are utilized together with $\mu_s = 0.75$, and $\mu_k = 0.4$ obtained experimentally; $k_{\mathrm{contact}} = 11.86$ N/mm, $c_{\mathrm{contact}} = 7.65 \times 10^{-3}$ N/(mm/s) are given. In order to rotate the object, we give to the plate's two DOFs of motion the following sinusoid trajectories

$$\Theta(t) = -A_p \sin(\omega_p t) \tag{10}$$
$$X(t) = B_p \sin(\omega_p t) \tag{11}$$

where A_p, B_p, and ω_p denote the rotational amplitude, the linear amplitude, and the angular frequency of the plate motion, respectively. Fig. 9 and Fig. 10 show the simulation result and the experimental result, respectively, with $A_p = 12$ deg, $B_p = 3$ mm, and $\omega_p = 12 \times 2\pi$ rad/s. From these figures, it can be seen that the dynamic behavior in simulation and that in the experiment qualitatively correspond to each other. Fig. 11 shows the relationship between the angular frequency of the plate ω_p and the angular velocity of the object ω_B deg/s in simulation and experiment, where ω_p is normalized by $\omega_n = 10\pi$ rad/s which is the first order natural angular frequency of the object in bending. It can be seen that the maximal angular velocity of the object is produced with $\omega_p/\omega_n = 2.8$ in both simulation and experiment. Here, it can be noted that the object's behavior changes with respect to ω_p. An interesting observation is that, if the whole object is separeted into two parts by its center, as shown in Fig. 9(a), and regarding each of these parts as left leg and right leg; then the object's behavior can be described with an analogy to human footsteps. These footsteps motions can be compared to the object's behaviors as follows: sliding (both legs always make contact with the floor), walking (at least one leg makes contact with the floor), and running (both legs float at the same time).[1] The change in these behaviors as ω_p increases can be observed in Fig. 11, and the maximal angular velocity is achieved in the running phase, which is also dynamically stable. Finally, for a larger ω_p, the object becomes unstable and it cannot rotate anymore. We define as

[1]The video attachment file of this paper shows experiments and the simulations illustrating the object's behaviors of rotation on the plate.

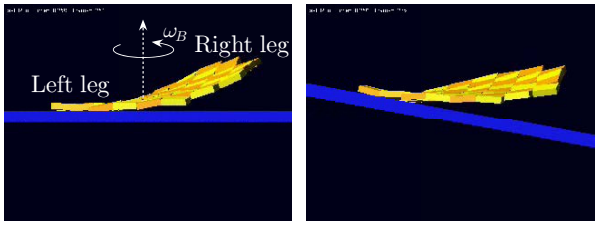

(a) $t = 0.0$ (b) $t = 0.014$

(c) $t = 0.028$ (d) $t = 0.042$

(e) $t = 0.056$ (f) $t = 0.069$

Fig. 9. Series of photos of the simulation using ω_p/ω_n = 2.4. The object is rotating on the plate with an angular velocity of $\omega_B = 350$ deg/s.

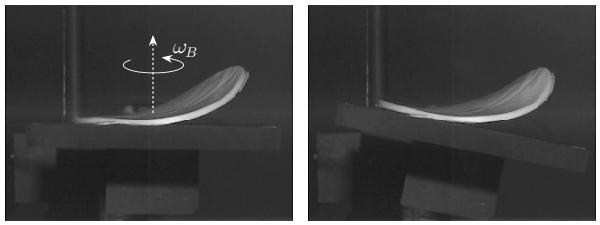

(a) $t = 0.0$ (b) $t = 0.014$

(c) $t = 0.028$ (d) $t = 0.042$

(e) $t = 0.056$ (f) $t = 0.069$

Fig. 10. Series of photos of the experiment using ω_p/ω_n = 2.4. The object is rotating on the plate with an angular velocity of $\omega_B = 370$ deg/s.

failures, those cases in which the object's center slips more than 10 mm or when the object turns over.

B. Optimum Plate Motion

The simulation results in Fig. 12 show the relationship between the rotational amplitude of the plate A_p, the angular frequency of the plate ω_p normalized by ω_n, and the angular velocity of the object ω_B. The dashed lines indicate the maximal ω_B for each A_p, projected onto the ω_p/ω_n-ω_B plane. If the robot can generate a high frequency of the plate e.g. ω_p/ω_n =5, the object will be able to rotate faster and stable with a small amplitude of the plate. It can be intuitively understood that a smaller amplitude contributes to the stability of the rotating object. From Fig. 12, the optimum combination of A_p and ω_p can be obtained, which leads to the maximal angular velocity of the object, under the given specification of the robot system. Fig. 13(a), (b), (c), and (d) show the relationship between the rotational amplitude of the plate A_p, the angular acceleration of the plate $A_p\omega_p^2$, and the angular velocity of the object ω_B, where the natural angular frequency of the object is: (a) $\omega_n = 3.5\pi$ rad/s, (b) $\omega_n = 10\pi$ rad/s, (c) $\omega_n = 33\pi$ rad/s, and (d) $\omega_n = 320\pi$ rad/s. The value of ω_n is changed by modifying the elasticity of the object for the same mass. In Fig. 13, □, △, and ◯ denote the object's sliding, walking, and running phases, respectively. As shown in Fig. 13(d), the object with the higher stiffness becomes unstable even with a low acceleration of the plate. Thus, the maximal angular velocity of the object ω_B is smaller than that of the softer objects in Fig. 13(a), (b), and

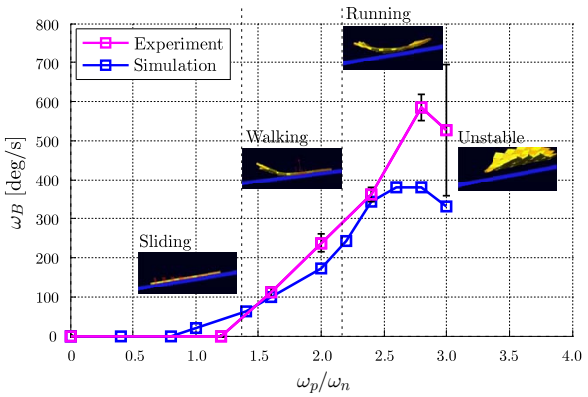

Fig. 11. Angular velocity of the object ω_B with respect to the angular frequency of the plate ω_p/ω_n.

(c). This corresponds to the experimental results as shown in Fig. 3 and Fig. 4. From Fig. 13(a), (b), (c), and (d), it can be confirmed that the optimum angular acceleration $A_p\omega_p^2$ is uniquely determined for each of the deformable objects, as indicated by the shaded area, while the maximal angular velocity of the object ω_B changes depending on how large the amplitude A_p is chosen. As shown in Fig. 13(b), (c), and (d), the maximal velocity of the object ω_B is produced in the running phase. This means that, to rotate the object faster, the plate needs an enough acceleration to push up the object so that it can run and turn. However, as shown in Fig. 13(a), the maximal velocity of the object is produced when walking. The reason is that the object is too soft, hence the object is greatly deformed, and as a result, it is folded in two before it

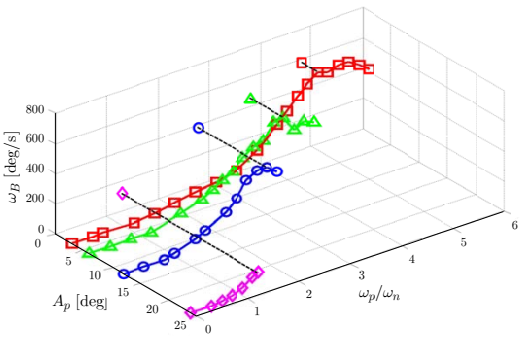

Fig. 12. Relationship between A_p, ω_p/ω_n, and ω_B.

starts to run. Thus, although the object's behavior differs, an appropriate angular acceleration of the plate is essential to generate a fast and stable rotation of the deformable object.

VII. Conclusion

This paper discussed a nonprehensile dynamic manipulation of a deformable object. The main results in this paper are summarized as follows:

1. We introduced a model for approximating the dynamic behavior of a deformable object, where the object is composed of multiple nodes and three DOFs joint units with viscoelasticity.
2. We showed how to estimate an object's viscoelastic parameters by experiment, and showed the simulation and experimental results to validate the introduced model. Dynamic behaviors in both simulation and experiment correspond to each other qualitatively.
3. We discovered through simulation analysis that the object's rotation behavior changes with respect to the plate frequency, similar to sliding, walking, and running motions done by human legs.
4. We obtained the optimum plate motion leading to the object's maximal rotational speed and revealed that the angular acceleration of the plate is essential for a dynamically stable and fast object rotation.

In the future, we would like to investigate friction's influence in the determination of the optimum plate motion as well as extend the analysis to thick objects so that we can apply it to several kinds of real deformable objects.

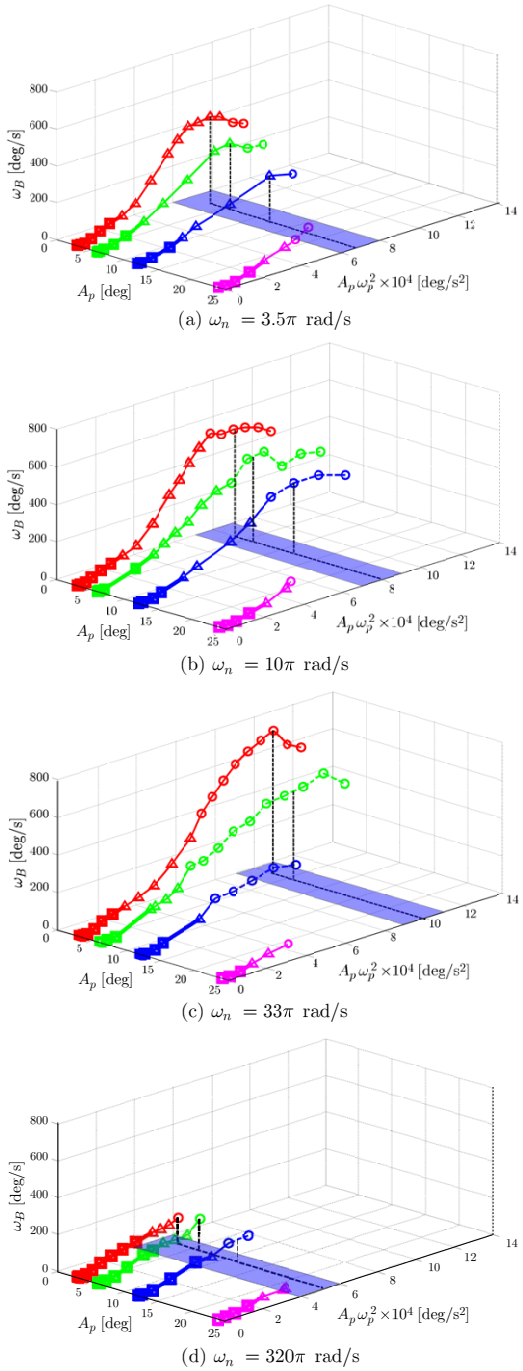

(a) $\omega_n = 3.5\pi$ rad/s

(b) $\omega_n = 10\pi$ rad/s

(c) $\omega_n = 33\pi$ rad/s

(d) $\omega_n = 320\pi$ rad/s

Fig. 13. Relationship between A_p, $A_p\omega_p^2$, and ω_B.

References

[1] H. Arai and O. Khatib: "Experiments with Dynamic Skills," Proc. of 1994 Japan-USA Symp. on Flexible Automation, pp.81–84, 1994.

[2] K. M. Lynch and M. T. Mason: Dynamic Nonprehensile Manipulation: Controllability, Planning, and Experiments, Int. J. of Robotics Research, vol.18, no.8, pp.64–92, 1999.

[3] A. Amagai and K. Takase: "Implementation of Dynamic Manipulation with Visual Feedback and Its Application to Pick and Place Task," Proc. of the IEEE Int. Symp. on Assembly and Task Planning, pp.344–350, 2001.

[4] M. Higashimori, K. Utsumi, Y. Omoto, and M. Kaneko: "Dynamic Manipulation Inspired by the Handling of a Pizza Peel," IEEE Transactions on Robotics, vol.25, no.4, pp.829–838, 2009.

[5] M. Higashimori, Y. Omoto, and M. Kaneko: "Non-grasp Manipulation of Deformable Object by Using Pizza Handling Mechanism," Proc. of the IEEE Int. Conf. on Robotics and Automation, pp.120–125, 2009.

[6] D. Reznik and J. Canny: "C'mon Part, Do the Local Motion!," In IEEE Proc. of the IEEE Int. Conf. on Robotics and Automation, pp.2235–2242, 2001.

[7] K. F. Böhringer, V. Bhatt, and K. Goldberg: Sensorless Manipulation Using Transverse Vibrations of a Plate, Proc. of the IEEE Int. Conf. on Robotics and Automation, pp.1989–1986, 1995.

[8] T. Vose, P. Umbanhowar, and K. M. Lynch: "Friction-Induced Velocity Fields for Parts Sliding on a Rigid Oscillated Plate," Proc. of the 2008 Robotics: Science and Systems Conf., 2008.

[9] K. Furutani, T. Higuchi, Y. Yamagata, N. Mohri: "Effect of Lubrication on Impact Drive Mechanism," Precision Engineering, vol.22, no.2, pp. 78–86, 1998.

[10] M. Moore, and J. Wihelms: "Collision Detection and Response for Computer Animation," Computer Graphics, vol.22, no.4, pp.289–298, 1988.